

**A NEW SENSOR BASED UPON A ROTATING-COIL  
ELECTROMAGNETIC INDUCTION CONCEPT  
SERDP Project MM-1447**

**FINAL REPORT**

AETC Incorporated  
Cary, NC

This report was prepared under contract to the Department of Defense Strategic Environmental Research and Development Program (SERDP). The publication of this report does not indicate endorsement by the Department of Defense, nor should the contents be construed as reflecting the official policy or position of the Department of Defense. Reference herein to any specific commercial product, process, or service by trade name, trademark, manufacturer, or otherwise, does not necessarily constitute or imply its endorsement, recommendation, or favoring by the Department of Defense.



# Contents

FIGURES .....	iv
TABLES .....	v
ACRONYMS .....	vi
1. Introduction.....	1
2. Extremely Low Frequency (ELF).....	2
3. Transmitter Coil.....	5
4. Receiver Coils and Preamplifier .....	13
5. Mechanical Design.....	18
6. Synchronous Detection (Lock-In Amplifier).....	20
7. System Integration and Tests .....	21
8. Summary .....	30
9. Future Research .....	31
10. References.....	32
APPENDIX A – DC Motor Control Specifications .....	33

## Figures

1. Calculated response (left) from solid and thin-walled cylinders oriented transverse to the transmitted primary field. Calculated responses (right) of 30 cm diameter spheres of varying thicknesses.....	2
2. Naturally occurring Shumann signals in the ELF region showing the primary resonant frequencies.....	3
3. The on-axis field due to the current in the loop.....	5
4. The field is measured by the magneto-meter at a distance of 97.8 cm from the transmitter coil along the centerline. The transmitter was operating at 2 amps DC.....	6
5. The transmitter coil is shown mounted on the rotating platform.....	6
6. Plot of the measured field (from the data in Table 1). The coil is rotating at 1 Hz with a current of 2 amp.....	7
7. Photograph showing the lower receiver coil situated 41.5 cm below the center of the transmitter coil.....	8
8. A plot of the primary receiver voltage measured at the preamp output.....	9
9. Receiver preamplifier and Tx coil position decoder schematic.....	10
10. Frequency response of the receiver preamp and coil.....	11
11. Complete motor control system and interconnections.....	12
12. The transmitter coil drive assembly is shown including the drive gearing, the motor, and the controller.....	12
13. Rotating electrical connector and wiring connections.....	13
14. Block diagram of the lock-in amplifier.....	14
15. Lower and upper receiver coils.....	15
16. Modeled flux linkage at 2 Hz for lower and upper receiver coils.....	15
17. Simulated residual voltage from lower and upper receiver coils.....	16
18. A solid steel metallic test object is shown lying horizontally under lower receiver coil.....	16

19. Rotating Coil System Block Diagram.....	17
20. Test results from Test 1 using the hollow and solid steel test objects .....	19
21. Results from Test 2 using the hollow and solid steel test objects in vertical and horizontal orientations.....	20
22. Test 3 results of hollow and solid responses.....	21
23. The GEM 3 sensor is shown mounted above the solid steel test object .....	22
24. Rotating coil system and GEM responses for the hollow steel test object .....	23
25. Rotating coil system and GEM responses for the solid steel test object .....	23
26. Comparison of multiple excitation angles of the primary magnetic field. Left side: Measurements are achieved by laterally traversing the sensor over the target while keeping the coil oriented horizontally to the target (red circle). The lower arrow shows the major component of the transmitted field observed by the target. On the Right Side the positions of both the sensor and the target remain fixed. The transmit and receive coils are rotated together above the target. The lower arrows again show the field observed by the target.....	26

## Tables

1. Measured transmitter field data .....	7
2. Experimental parameters and measured induced voltages .....	8
3. Measured response of the receiver coil and preamplifier .....	11
4. Specifications of a Model 430 rotating electrical connector .....	13
5. Data from the first experimental test setup .....	19
6. Data from the second experimental test setup .....	20
7. Data from the third experimental test setup.....	21

# Acronyms

# 1. Introduction

The research described in this report was conducted in support of SERDP SEED Broad Agency Announcement (BAA) dated November 7, 2003, Statement of Need UXSEED-05-01, which specifically called for development of new UXO sensors at the proof-of-concept level that will allow development of new or improved discrimination techniques for distinguishing intact ordnance from metallic scrap items.

Modern UXO geophysical surveys are normally conducted under GPS control using arrays of magnetometers and/or EMI sensors. Typical vehicular towed arrays produce high density maps of 200,000 – 2,000,000 data points per acre when using EMI and magnetometer sensor arrays. Target analyses typically involve fitting of perceived magnetic anomalies to dipole signature models. To improve the ability to distinguish intact UXO from metallic scrap, statistical analysis approaches often are applied to the output parameters of the physics-based target-fitting algorithms to improve the classification ability. Although we can approach the 100% detection of UXO threats on fairly uncomplicated ranges, clearing the ranges still requires digging 5-25 non-UXO targets to recover each intact UXO. We have recently concluded that, using currently available magnetic and EMI sensors, little or no further performance gain is likely to be achieved using only the physics-based fitting parameters to make decisions about ordnance classification. Frequency-domain EMI sensors such as the GEM-3<sup>TM</sup> from Geophex Ltd. can operate at frequencies as low as 30 Hz. However, the signal-to-noise ratio of measurements at frequencies below 100 Hz is significantly degraded.

The objective of the project was to demonstrate that an Extremely Low Frequency (ELF) EMI sensor employing a rotating transmitter coil can be used to efficiently measure inphase and quadrature responses of buried metallic targets in the frequency range between 1 and 30 Hz. The transmitter coil employs a DC magnetic field, which when rotated about one of its primary axes, effectively produces a sinusoidal time-varying magnetic field. This approach overcomes several limitations of existing frequency domain EMI sensors that prevent their effective use at frequencies below 100 Hz. We describe in this report the design of a laboratory prototype rotating-coil EMI system with a transmitter coil, receiver coils, receiver preamplifier and a lock-in amplifier for processing of the preamplifier signal output into inphase and quadrature components. We report data measurements from various targets at individual frequencies and show the data plots.

## 2. Extremely Low Frequency (ELF)

It is our premise that significant additional information pertaining to the shape and identity of metallic objects can be derived from measurements in the ELF region. This possibility has been explored by Kevin O'Neill,<sup>1</sup> as shown graphically in the plots of Figure 1.

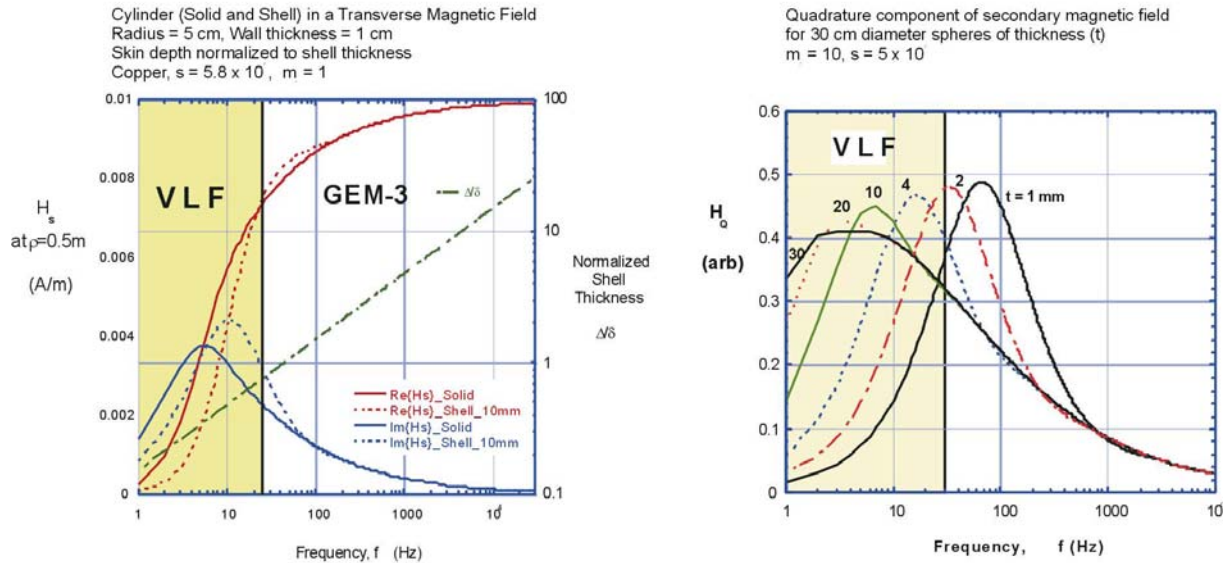


**Figure 1.** Calculated response (left) from solid and thin-walled cylinders oriented transverse to the transmitted primary field. Calculated responses (right) of 30 cm diameter spheres of varying thicknesses.

Measurements made below 25-30 Hz (in the frequency region designated as VLF (Very Low Frequency) in these plots) show that signal differences between solid and thin-walled objects often appear only at frequencies below 30 Hz. Although these plots are for non-ferrous objects, real-world UXO often are characterized by quadrature component signals that peak in this region. Due to signal-to-noise limitations of existing equipment, when taking readings at these low frequencies it is normally necessary to maintain the equipment in a static location and acquire many minutes (possibly hours) of data to allow stacking and averaging to extract a measurable signal from the noise. This method yields better results but inherently is very time consuming.

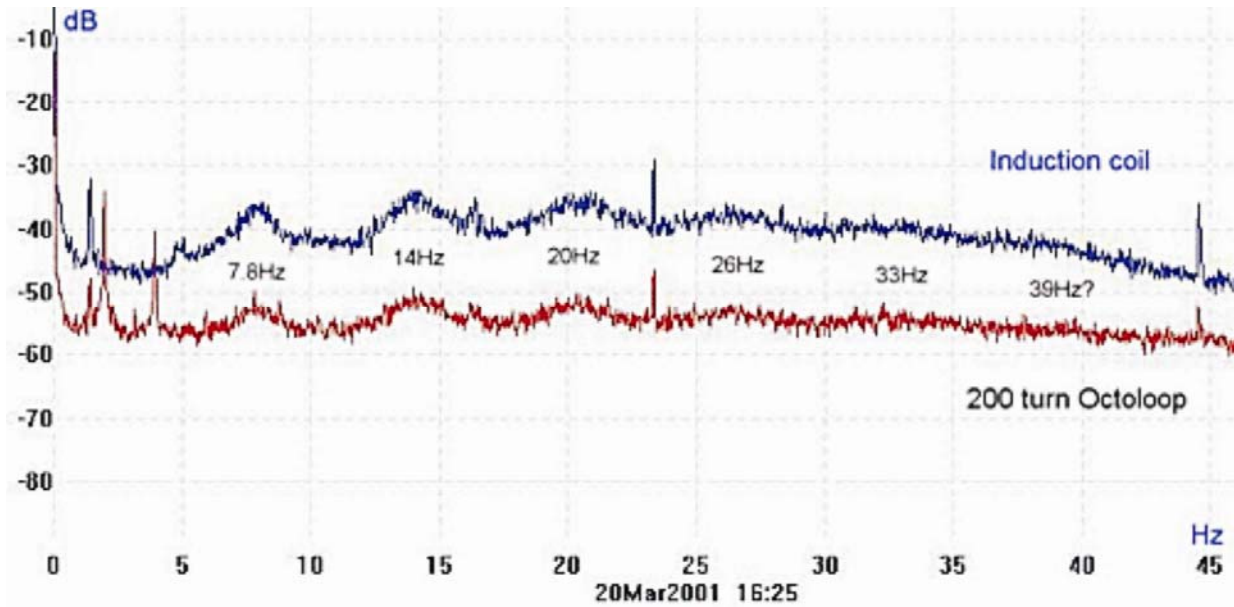


**Figure 2.** Naturally occurring Shumann signals in the ELF region showing the primary resonant frequencies.

One phenomenon that produces interference at these low frequencies is Shumann Resonances. These EM signals that are generated by natural causes such as lightning strikes occur at fixed frequencies in the ELF range of frequencies. The resonances (**Figure 2**) result from the signals propagating around the earth bouncing in waveguide-like fashion between the Earth's surface and the ionosphere. In our project, the horizontal co-planar orientation of the receiver coils will tend to minimize their interference because their propagation vector is primarily parallel with the Earth's surface. Our transmitter coil and its developed moment should overcome the Shumann<sup>2</sup> signals that may be present at the receiver coils.

### 3. Transmitter Coil

The transmitter coil was selected to be 100 turns of AWG # 20 copper magnet wire. The transmitter coil diameter is 20 cm, the width is 2.54 cm and the thickness is 0.64 cm. The calculated inductance (L) of the transmitter coil is shown below:

$$\text{Eq.1} \quad L = \frac{0.8 (rN)^2}{6r + 9l + 10b} \quad \text{where: } r = \text{radius (inches)}$$

$$l = \text{width (inches)}$$

$$b = \text{height (inches)}$$

$$N = \text{number of turns}$$

The calculated inductance of the coil is:

$$L = \frac{0.8(3.94 \times 100)^2}{6(3.94) + 9(1) + 10(.25)} = 3.53 \text{ mH}$$

-the measured inductance of the transmitter coil is 3.39 mH. This is within 5% of the calculated value.

We tested the “rotating transmitter coil” using two different coil currents: 1 and 2 amp DC. The transmitted moments at 1 and 2 amps are given by:

$$m(\text{Tx}) = NIa \quad \text{where: } N = \text{number of turns}$$

$$I = \text{current flowing in the coil}$$

$$a = \text{area of one turn } (\pi r^2)$$

Therefore, the transmit moments are:

1 Amp	2 Amp
$100(1 \text{ Amp})(0.031) = 3.14 \text{ Am}^2$	$100(2 \text{ Amp})(0.031) = 6.28 \text{ Am}^2$

The arrangement shown in Figure 3 was used to determine the magnetic field (B) along the axis of the transmitter loop. The field is given by:

$$\text{Eq. 2} \quad B = \frac{\mu_0 I r^2}{2\sqrt{(r^2 + x^2)^3}} \quad \text{where: } \mu_0 = 1.26 \times 10^{-6} \text{ H/m}$$

$$I = \text{effective current (amps)}$$

$$r \text{ and } x \text{ are shown in Figure 3}$$

When  $x \gg r$  Eq. 2 can be simplified to:

$$\text{Eq.3 } B = \frac{\mu_0 I r^2}{2 x^3}$$

which is equivalent to the expression for on axis magnetic field due to a magnetic dipole:

$$\text{Eq.4 } B = \frac{\mu_0 I A}{2\pi x^3} \quad \text{where } A \text{ is the area of the current loop, } \pi r^2$$

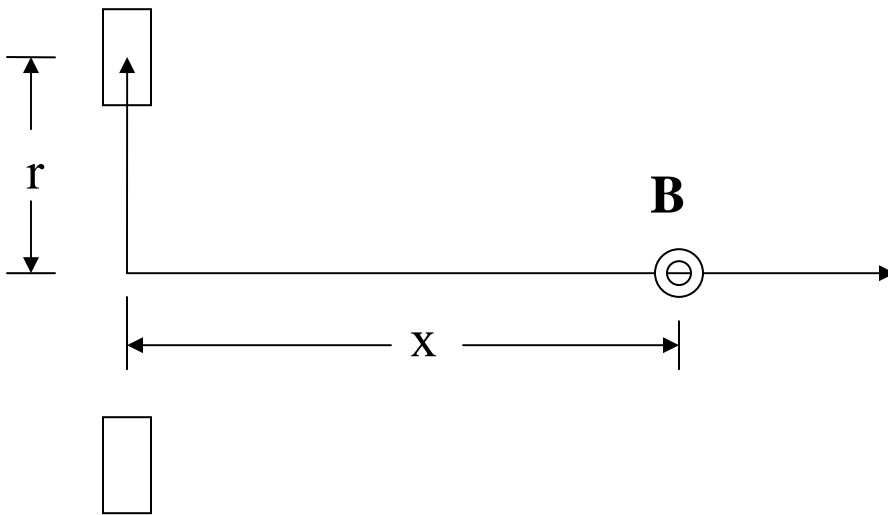


**Figure 3. The on-axis field due to the current in the loop.**

We used a Cesium Vapor total field magnetometer to measure the magnetic field developed by the transmitter coil. The magnetometer center was set at a distance of 38.5 inches away from our transmitter coil center. Thus referring to Figure 3,  $x = 0.972$  m and  $r = 0.1$  m. Substituting these distances along with a transmitter current of 2 Amps into Eq. 4 gives:

$$B = \frac{(1.26 \times 10^{-6})(200)(0.0314159)}{2\pi (0.972)^3} = 1,372 \text{ nT}$$

The equipment was set up and measurements taken to compare the calculated value (1372 nT) with the measured value. The transmitter current was repeatedly turned on and off during the experiment to measure the change in the earth's magnetic field at the total field magnetometer. This data are shown in Figure 4.

From Figure 4 we can see that the measured offset field is 1260 nT, which compares closely (within 10%) with the calculated value of 1372 nT.

We then mounted the transmitter coil onto our rotating platform as shown in Figure 5.

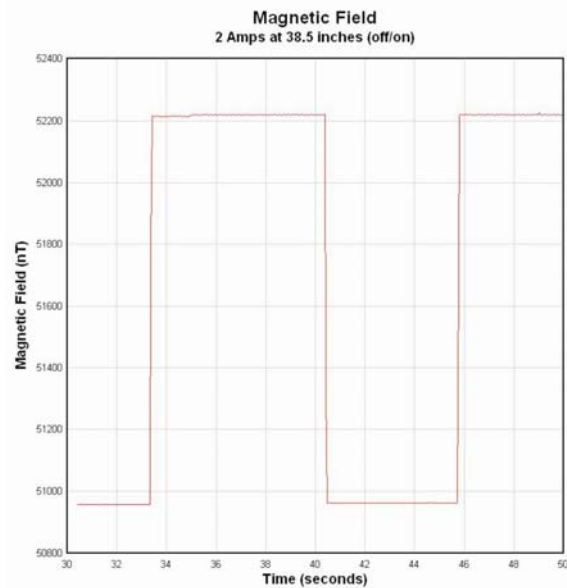


**Figure 4.** The field is measured by the magnetometer at a distance of 97.8 cm from the transmitter coil along the centerline. The transmitter was operating at 2 amps DC.



**Figure 5.** The transmitter coil is shown mounted on the rotating platform.

The transmitter coil was set to rotate at 60 RPM (1 Hz). The magnetometer (set up in the same position used in Figure 4) was used to measure the time-varying field. A 2-second clip of Data are shown in Table 1 and plotted in Figure 6.

**Table 1. Measured transmitter field data**

nT	Time
52198.68	41.906
52229.90	41.953
52141.85	42.000
51947.10	42.046
51656.67	42.093
51296.74	42.156
50896.29	42.203
50498.05	42.250
50149.03	42.296
49885.86	42.343
49725.30	42.406
49678.62	42.453
49752.09	42.500
49945.64	42.546
50252.29	42.593
50644.48	42.656
51074.71	42.703
51487.44	42.750
51841.99	42.796
52090.20	42.843
52217.43	42.906
52218.33	42.953
52108.10	43.000
51889.27	43.046
51579.74	43.093
51200.62	43.156
50791.14	43.203
50400.80	43.250
50069.87	43.296
49831.17	43.343
49700.95	43.406
49684.12	43.453
49790.17	43.500
50012.39	43.546
50343.36	43.593
50751.95	43.656
51182.04	43.703
51585.92	43.750
51915.33	43.796
52131.97	43.843
52228.63	43.906
52203.54	43.953

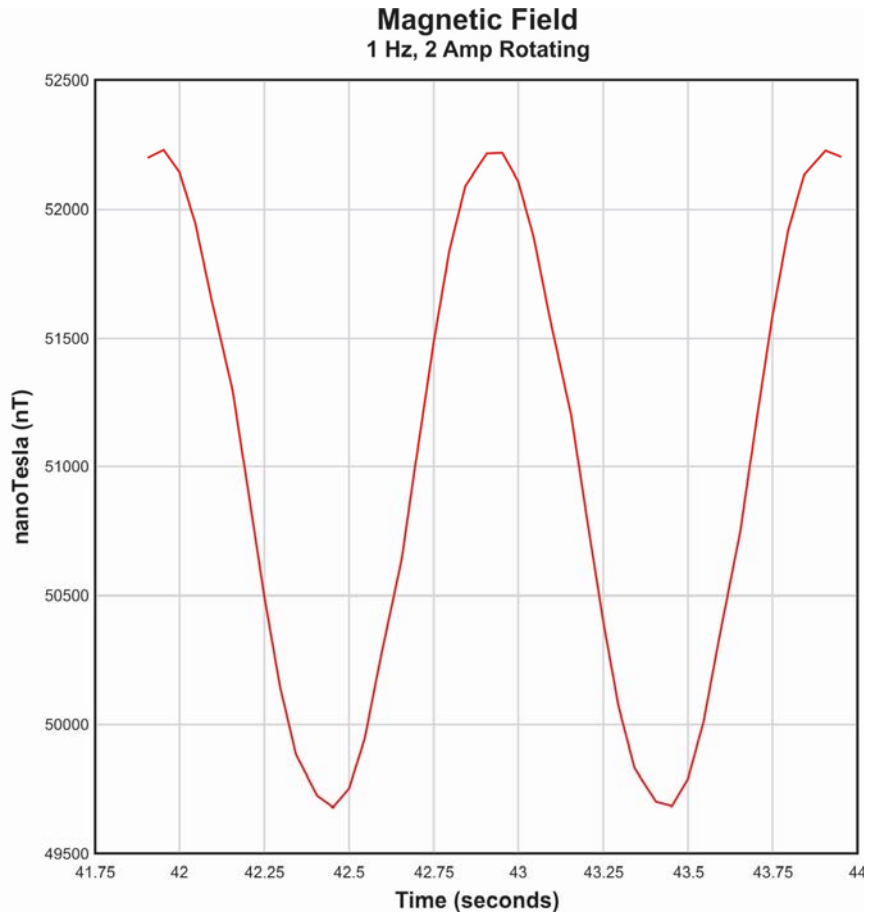


**Figure 6. Plot of the measured field (from the data in Table 1). The coil is rotating at 1 Hz with a current of 2 amp.**

We see from **Figure 6** that the measured sinusoidal magnetic field oscillates 2,520 nT peak-to-peak (1260 nT peak above and below the Earth's background field of 50,960 nT).

## 4. Receiver Coils and Pre-amplifier

The receiver coils were wound on coil formers made of the same plastic material as the transmitter coil and had the same diameter (20 cm) and width (2.54 cm) as the transmitter coil. The receiver coils were wound with 500 turns of AWG #22 magnet wire. Their DC resistance was measured as 43 ohm. Tests were first performed with the setup shown in Figure 7, with only one receiver coil situated 41.5 cm below the transmitter coil center. This distance was chosen to allow use of existing non-metallic shelving rather constructing specialized jigs to fit the coils to a fractional meter spacing.

A series of calculations were conducted to determine the induced receiver coil voltage (receiver coil pickup) using different transmitter currents, differing number of turns on the receiver coil, different transmitter-receiver distances and different coil dimensions. The results are shown in spreadsheet format in Table 2.

The receiver preamplifier was used to amplify the small receiver coil induced voltages to a level appropriate for synchronous detection. In general, gains were set to produce a signal of 1 volt (peak-to-peak). This level provides a good signal to noise ratio (SNR) typically swamping out Schumann Resonances, and radiated noise associated with other sources in the laboratory. We chose a current rather than a voltage amplifier. It terminates the receiver loops into a virtual short circuit (negative input of the op-amp). The op-amp is biased half way between ground and the power supply by a voltage divider network formed by R4 and R5. This allows the voltages to swing bi-polar about the bias point. C5 and C6 are used to block the DC bias voltages and L1 is used to reject high frequency RF signals associated with the laboratory background. The gain of this type of amplifier is equal to the feedback impedance divided by the input impedance. From **Figure 9** the feedback impedance is  $R3 \parallel C4$  ( $R3$  in parallel with  $C4$ ). At 1 Hz this

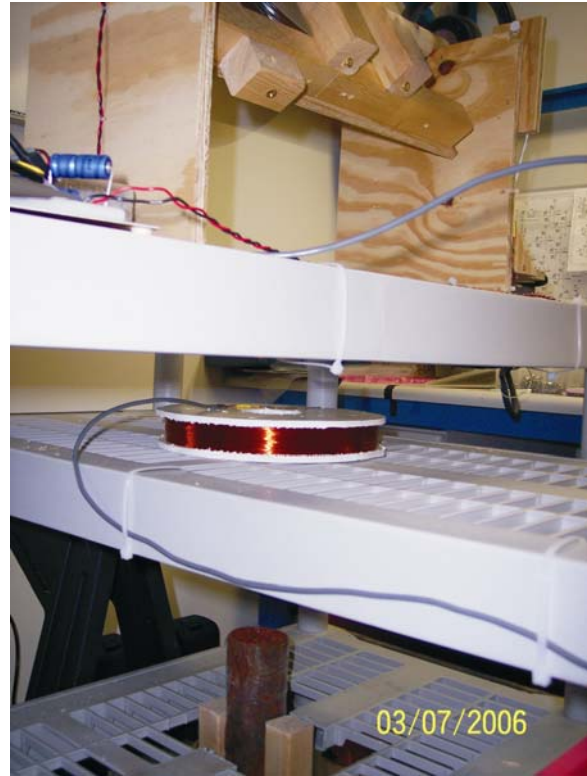


**Figure 7.** Photograph showing the lower receiver coil situated 41.5 cm below the center of the transmitter coil.

**Table 2.** Experimental parameters and calculated induced voltages

Receiver Coil Diam. (m)	Receiver Coil Turns	Receiver NA (Calculated)	Rotation Frequency (Hz)	Distance (m)	Transmit Coil Diam. (m)	Transmit Coil Turns	Trans. NA	Trans Current amp (rms)	Receiver Induced Voltage (rms)
0.2	500	15.71	1	0.50	0.2	100	3.1416	0.707	0.000351
0.2	500	15.71	1	0.27	0.2	100	3.1416	1.414	0.004455
0.2	500	15.71	1	0.27	0.2	200	6.2832	0.707	0.004455
0.2	500	15.71	1	0.25	0.2	100	3.1416	0.707	0.002806
0.2	500	15.71	1	0.42	0.2	100	3.1416	1.414	0.001227

calculates to be 320K. The input impedance is  $43 + 52 + 72(X_{C6}) = 167$ , therefore the circuit gain is  $320K / 167 = 1,916$ . From **Table 2** at 1 Hz it can be found that the receiver coil voltage pickup (Vpu) is calculated as 1.23 mV (rms). When we multiply this voltage pickup by our circuit gain, the circuit output voltage is calculated to be 2.35 V (rms) or 3.32 V (pk).

**Figure 8** shows the measured primary voltage at 1 Hz as ~3.0 V (pk), which is within 10% of our calculated value of 3.32 V (pk). This voltage parameter is also known as 1,000,000 ppm as it is the voltage due to the full primary transmitted field at the receiver coil. All secondary voltages (due to metallic anomalies) are compared to this primary voltage and expressed in units of ppm.

Measurements in this study are reported as voltages rather than the ppm values used by instrument manufacturers.

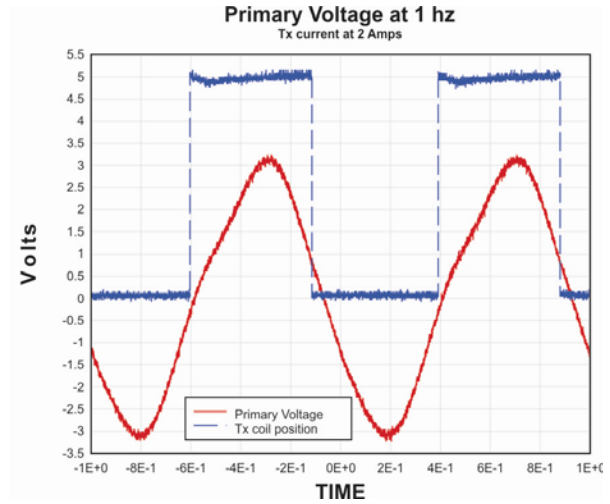
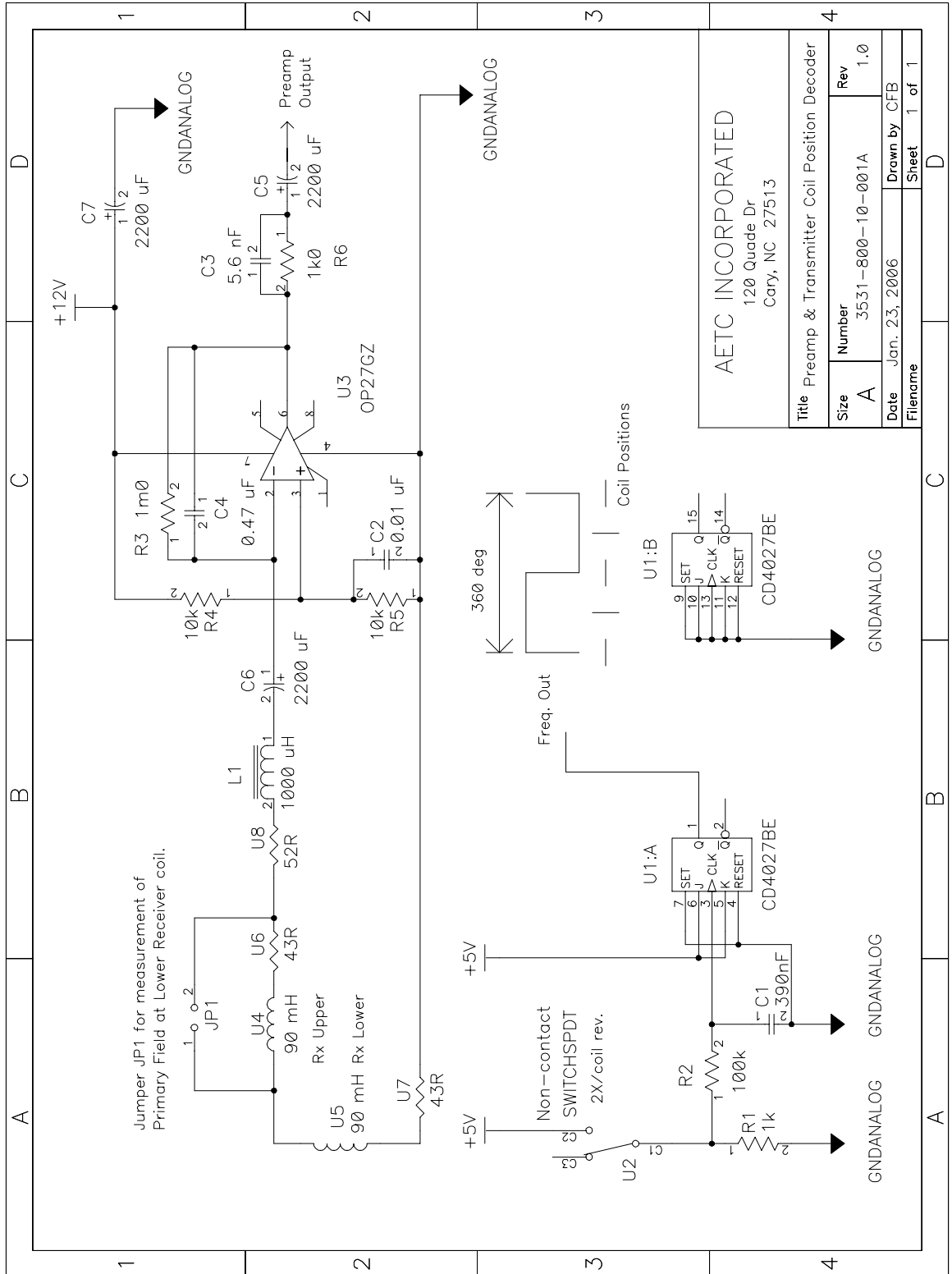


**Figure 8.** A plot of the primary receiver voltage measured at the preamp output.



AETC INCORPORATED  
120 Quade Dr  
Cary, NC 27513

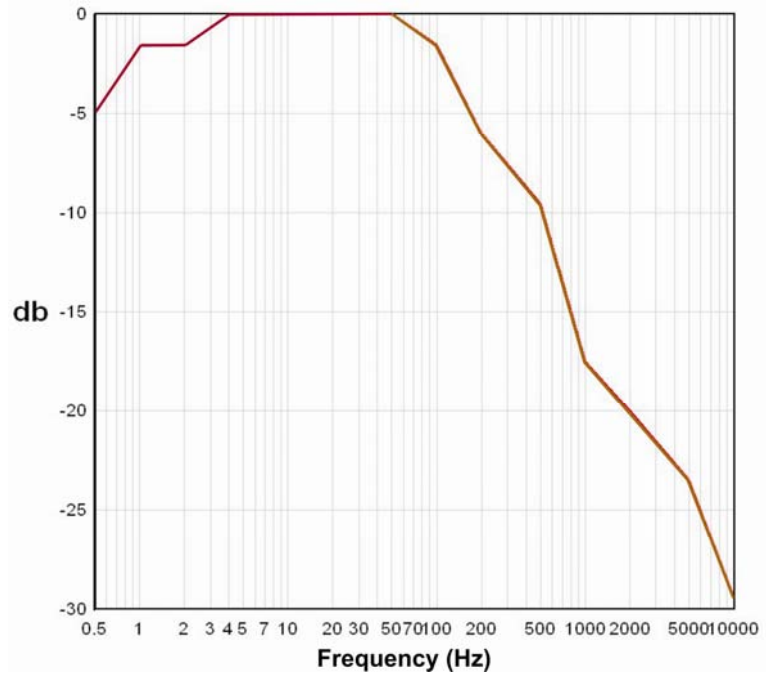
Title		Rev	
Preamp & Transmitter Coil Position Decoder		A	1.0
Size	Number	Date	Drawn by
A	3531-800-10-001A	Jan. 23, 2006	CFB
Filename			Sheet
			1 of 1

Figure 9. Receiver preamplifier and Tx coil position decoder schematic.

The frequency response of the receiver coil coupled to the receiver preamplifier was measured. The results are shown in **Table 3**. This receiver has a flat (0 db) response from 4-50 Hz. There is only -1.58 db attenuation at 1 Hz and -4.93 attenuation at 0.5 Hz. **Figure 10** shows a plot of the measured frequency response.

**Table 3. Measured response of the receiver coil and preamplifier**

Freq (Hz)	Vout (mV)	db
0.5	85	-4.9
1	125	-1.6
2	125	-1.6
4	150	0.0
8	150	0.0
10	150	0.0
20	150	0.0
50	150	0.0
100	125	-1.6
200	75	-6.0
500	50	-9.5
1000	20	-17.5
2000	15	-20.0
5000	10	-23.5
10000	5	-29.5



**Figure 10. Frequency response of the receiver preamp and coil.**

## 5. Mechanical Design

The mechanical design of the system is built around the selected control motor. A DC drive motor is the best design for this application. We selected was a Brushless DC motor with a variable speed control unit. This control unit is designed to precisely control motor shaft speeds of 100-2000 RPM. The motor control system and interconnections are shown in **Figure 11**.



**Figure 11. Complete motor control system and interconnections.**

Drive ratios were chosen to achieve the required transmitter coil RPMs and pulleys were acquired with the appropriate gear tooth ratios. A geared drive belt was ordered and the driver system assembled as shown in **Figure 12**.

Once the drive system design was completed, a method of achieving a constant electrical connection to the rotating transmitter coil had to be designed and implemented. Normally in this type of application slip-rings are used. However, this approach employs carbon brushes, in which the resistance of the contacts can vary. We chose an alternative approach. This method uses a rotating electrical connector with a unique design in which the electrical conduction path is a liquid metal that is molecularly bonded to the contacts. These connectors exhibit very low resistance (<1 milliohm) and have near zero electrical noise.



**Figure 12. The transmitter coil drive assembly is shown including the drive gearing, the motor, and the controller.**

**Figure 13** shows the rotating connector and the wiring harness. The specifications are shown in **Table 4**.

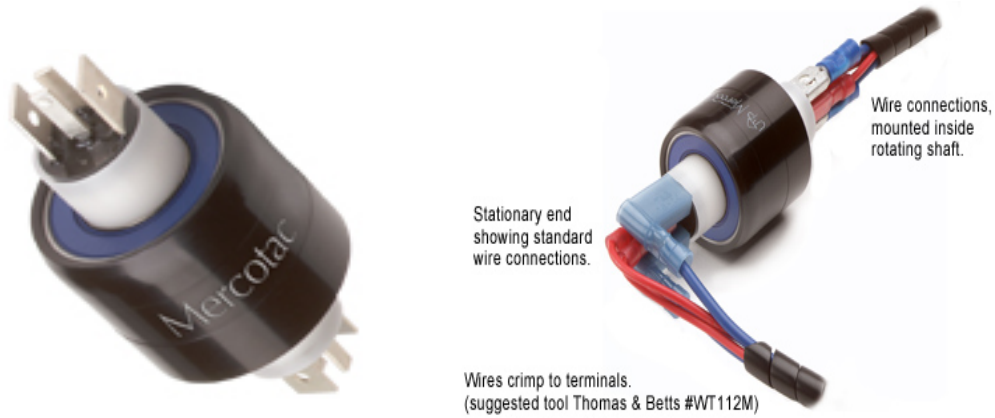


**Figure 13. Rotating electrical connector and wiring connections.**

**Table 4. Specifications of a Model 430 rotating electrical connector**

Model No.	Terminals	Voltage AC/DC	Amp Rating @240VAC	Max. Freq. MHz	Contact Resistance	Max. RPM	Temp Max. F (C) / Min. F (C)	Rotation Torque (gm-cm)	Circuit Separation
430	4	0-250	2@4/2@30	100	<1m $\Omega$	1200	140 (60) /-20(-29)	400	>25M $\Omega$
430-SS	4	0-250	2@4/2@30	100	<1m $\Omega$	1200	140 (60) /-20(-29)	400	>25M $\Omega$

The remaining mechanical item to be developed was a method of determining the transmitter coil position. The position must be known to produce a reference signal for the synchronous detector described in **Section 6**. The position was determined by using non-contact switches at each horizontal position and using these positions to generate a digital signal that toggles with each 180 degrees of rotation. The electrical schematic and coil position description is shown in **Figure 9** as the position decoder.

## 6. Synchronous Detection (Lock-In Amplifier)

The lock-in amplifier is used for two primary purposes; to recover signals in the presence of noise and/or to provide high resolution measurements of relatively clean signals over several orders of magnitude or intensity and frequency. A lock-in amplifier accepts an AC voltage input and provides a DC voltage output that is proportional to the input AC signal. This is schematically shown in **Figure 14**.<sup>3</sup>

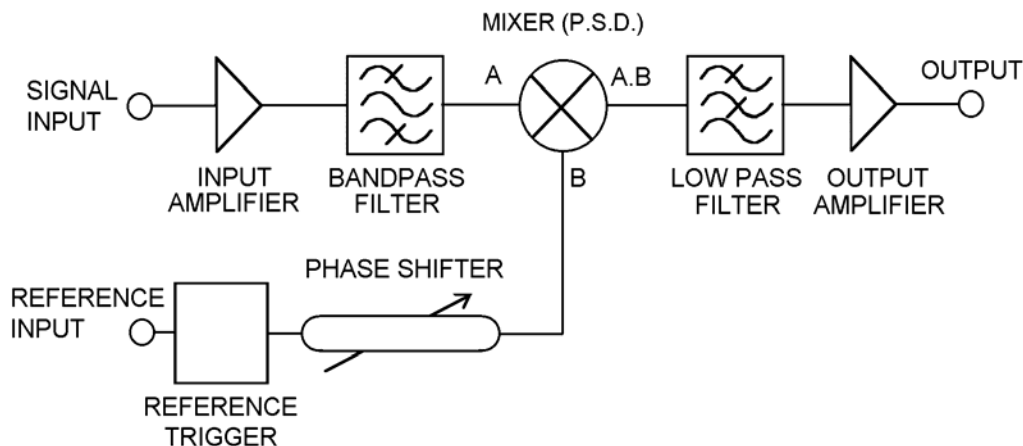


**Figure 14.** Block diagram of the lock-in amplifier.

This AC to DC conversion is performed by a phase-sensitive detector (PSD). It rectifies only the signal of interest while suppressing the noise or interfering signal components that may accompany the signal. To function correctly, the rectifier must be programmed to recognize the signal of interest. This is done by providing it with a reference voltage of the same frequency and with a fixed phase relationship to the signal. This is most commonly done by ensuring that the signals are derived from the same source. In our case, the signal (Receiver coil voltage) and the reference (Transmitter coil position) are derived from the same rotating transmitter coil mechanism. Using this reference signal allows the lock-in amplifier to track changes in the frequency of the signal of interest, since the circuit is “locked” to it. Dual phase lock-in amplifiers have a second PSD that is 90 degrees shifted with respect to the other PSD; the second PSD produces a quadrature (Y) output while the original PSD outputs the inphase (X) signal. Each PSD is followed by a low pass filter to eliminate any remaining AC components in the output signal. This leaves only a pure DC voltage output representative of the input signal. The lock-in amplifier used for this project was an Ametek Model 7225 DSP.

## 7. System Integration and Tests

Once tests were satisfactorily completed using the single lower receiver coil, the upper receiver coil was added. **Figure 15** shows them deployed at equal distances above and below the transmitter coil.



**Figure 15.**  
Lower and upper receiver coils.

Modeling of the electromagnetic performance of our system was performed utilizing Ansoft's Maxwell 3D Electromagnetic Simulation Software. **Figure 16** shows the modeled flux linkage at 2 Hz.

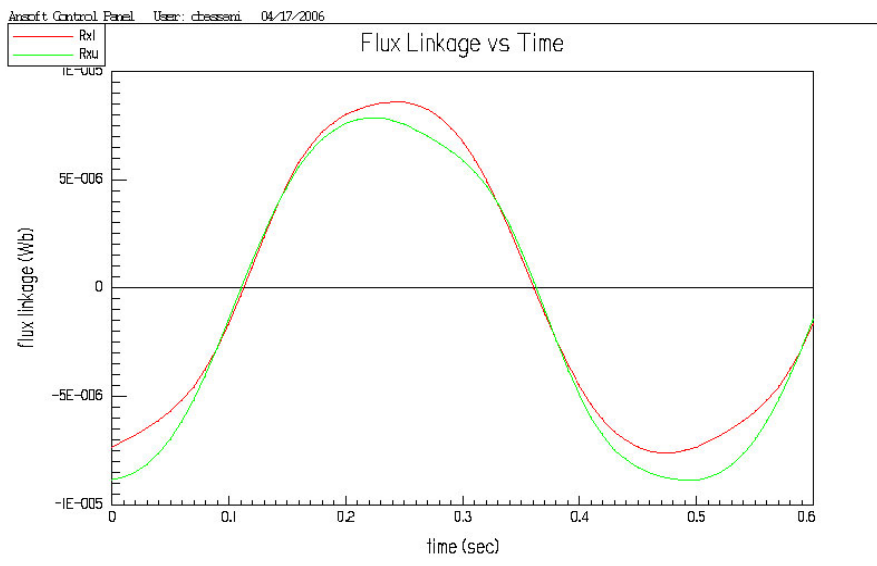


**Figure 16.**  
Modeled flux linkage at 2 Hz for lower and upper receiver coils.

The two receiver coils (lower and upper) were connected in series as shown in **Figure 9** so that the induced voltages were opposing, canceling each other. This resultant voltage after nulling is typically called the **residual voltage**. It is shown in **Figure 17** as simulated by the modeling software.

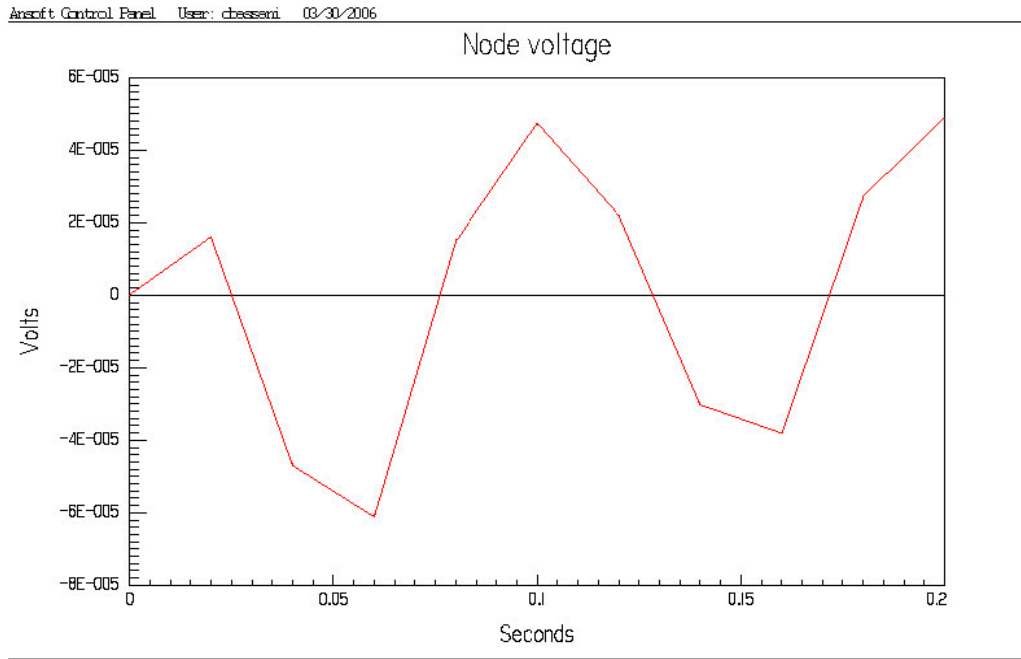


**Figure 17. Simulated residual voltage from lower and upper receiver coils.**

This simulated residual voltage is approximately  $5 \times 10^{-5}$  V (peak). The original primary voltage was approximately 3 V(peak). Our primary voltage has thus been reduced by -95.6 db. Test procedures were designed and various metallic objects were positioned under the lower receiver coil as shown in **Figure 18**. The complete rotating coil system was connected as shown in **Figure 19**.

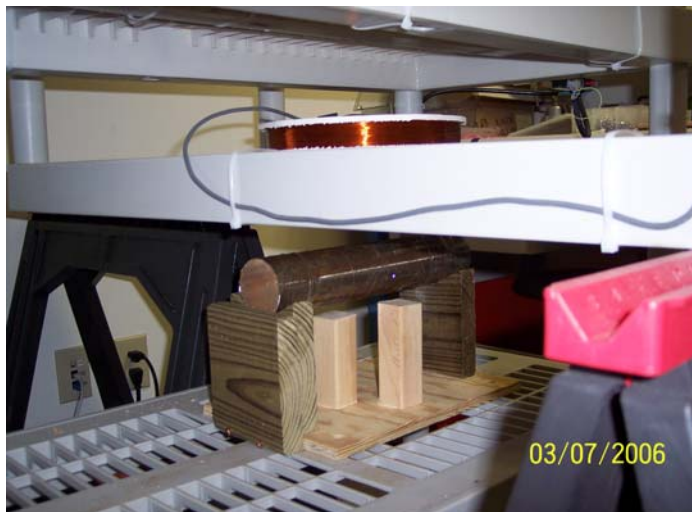


**Figure 18. A solid steel metallic test object is shown lying horizontally under lower receiver coil.**

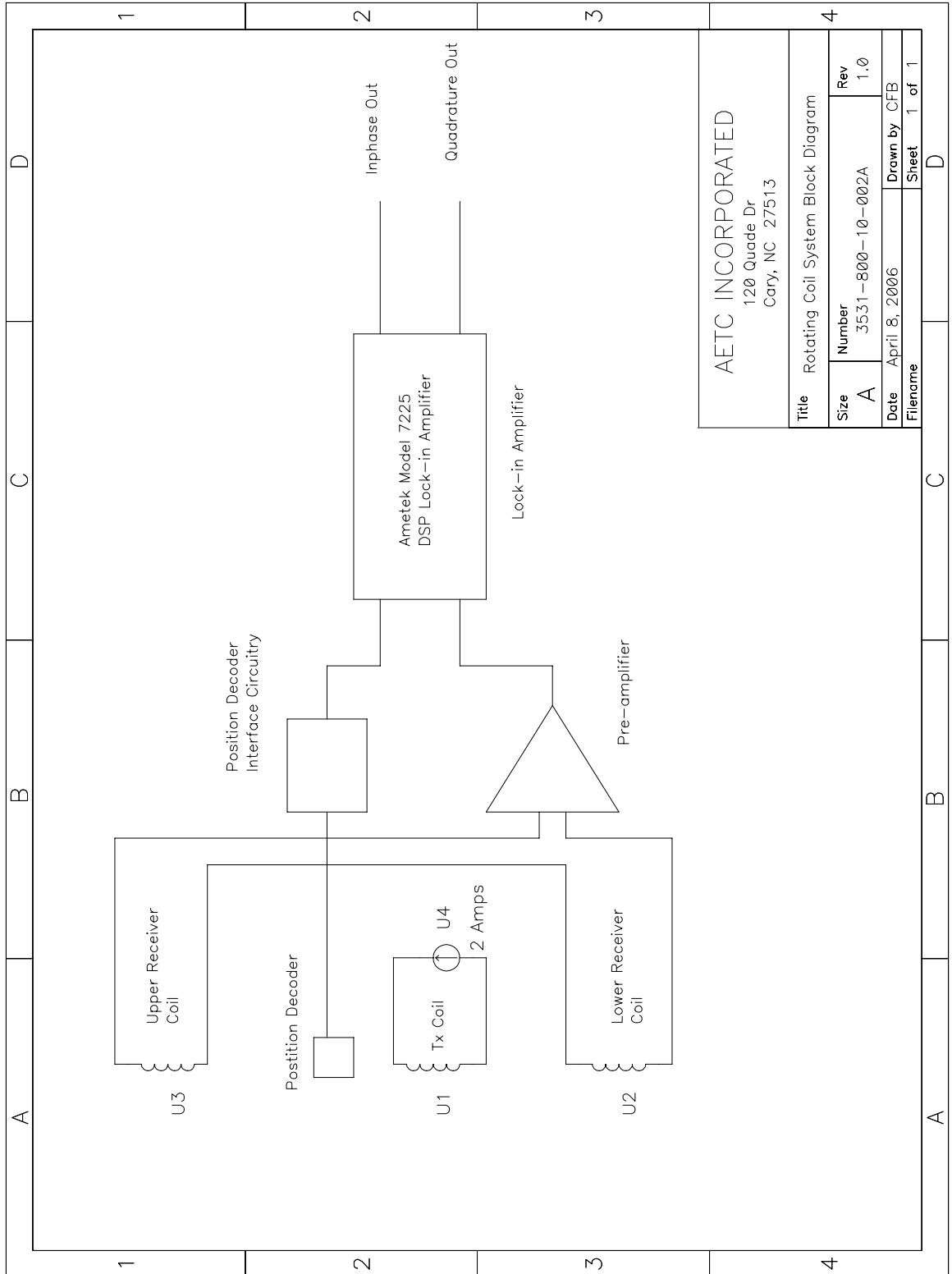


**Figure 19. Rotating Coil System Block Diagram.**

Each set of experimental measurements that we conducted, followed the same procedure:

- 1) The transmitter coil was set to rotate at the desired speed,
- 2) The output voltages were nulled at the lock-in,
- 3) A ferrite rod was placed under the lower receiver coil (to maximum coupling),
- 4) The Phase of the lock-in amplifier was adjusted so that the response was all inphase,
- 5) The ferrite rod was removed,
- 6) The output voltages were again nulled,
- 7) The metallic test object was placed in position in the jig,
- 8) The output voltages were recorded,
- 9) The test object was removed, and
- 10) The output voltages were again recorded (to measure short term drift).

The lock-in amplifier was used with the following parameter settings:

- 1) AC voltage gain = 20 db
- 2) Output time constant = 5 seconds
- 3) Output low pass filter rolloff = 24 db/octave

The metallic test objects were:

- 1) A 12-in long x 2.375-in diameter solid steel rod
- 2) A 12-in long x 2.375-in diameter (OD) hollow steel pipe (with a 0.125-in wall)

The solid steel rod (see **Figure 18**) was mechanically sawed from a longer rod. The ends were raw saw cuts. The sides had a rust coating. No attempt was made to clean up the test object or to smooth or polish its surfaces. The hollow steel test object was a piece of galvanized steel pipe that was sawed from a longer piece of pipe. The ends of the pipe were closed by galvanized pipe caps. No attempt was made to clean, smooth, or polish the test object.

Test 1 was conducted with the solid and hollow steel test objects in the Horizontal orientation only. The data are shown in **Table 5** and graphically presented in **Figure 20**.

**Table 5. Data from the first experimental test setup**

FREQ(Hz)	SOLID			HOLLOW		
	Real	Imaginary	Q	Real	Imaginary	Q
1	38.81	3.55	10.932	39.05	2.275	17.165
2	40.15	9.1	4.412	43.46	1.69	25.716
4	45.45	10.52	4.320	43.81	5.07	8.641
6	55.39	15.76	3.515	43.13	12.05	3.579
8	46.69	38.06	1.227	46.86	4.42	10.602
9	29.75	18.43	1.614	45.59	11.72	3.890
10	30.08	15.17	1.983	44.58	16.88	2.641
12	38.41	11.89	3.230	45.66	15.58	2.931

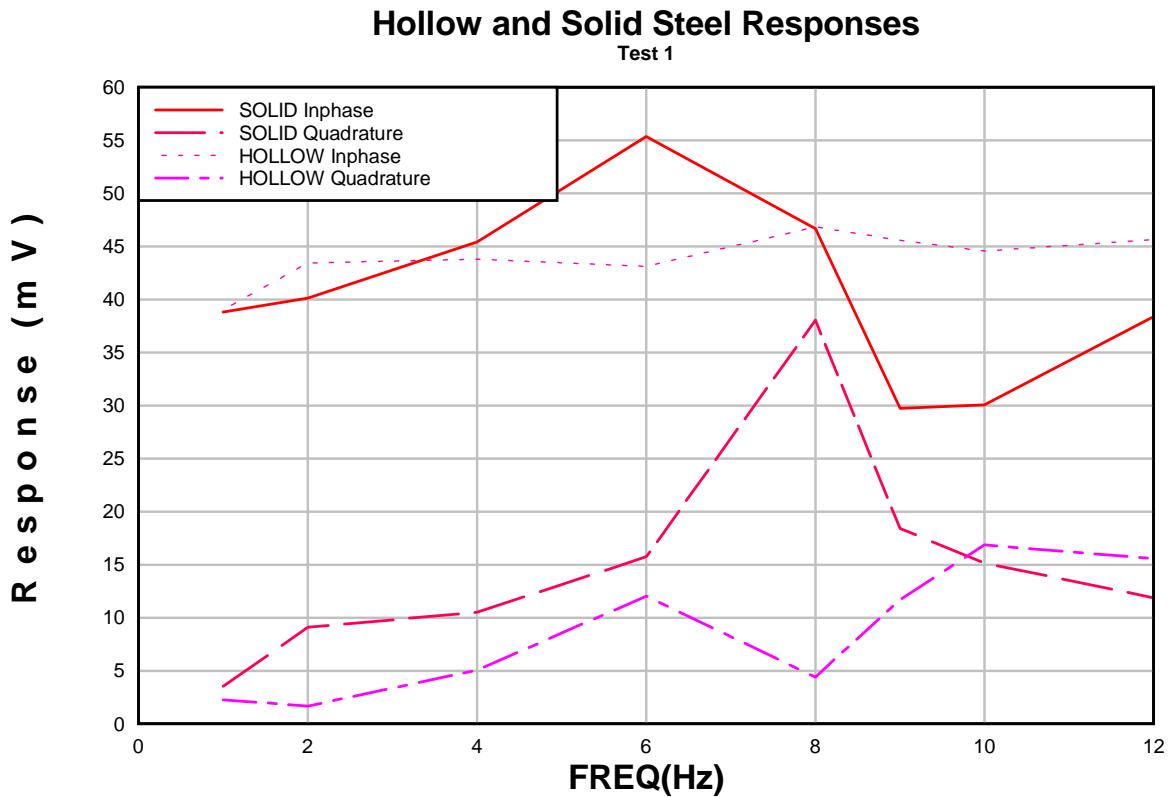


**Figure 20. Test results from Test 1 using the hollow and solid steel test objects.**

Test 2 was conducted with the solid and hollow steel test objects in both Horizontal (H) and Vertical (V) orientations. The data are shown in **Table 6** and graphically presented in **Figure 21**.

**Table 6. Data from the second experimental test setup**

FREQ (Hz)	SOLID (Horo)		HOLLOW (Horo)		SOLID (Vert)		HOLLOW (Vert)	
	Real	Imaginary	Real	Imaginary	Real	Imaginary	Real	Imaginary
1	33.6	2.11	29.33	1.63	20	0.34	16.7	2.4
2	37.11	0.99	34.17	0.57	19.65	3.53	16.63	0.22
4	44.96	0.37	34.22	4.51	19.1	1.76	16.46	1.68
6	34.46	19.05	36.83	2.74	17.92	5.44	16.57	1.9
8	49.44	25.44	35.33	1.63	17.16	6.11	16.41	2.52
10	40.12	11.47	35.79	1.55	15.92	5.89	16.16	2.47
12	36.66	4.44	36.85	3.26	15.25	4.44	15.95	2.81

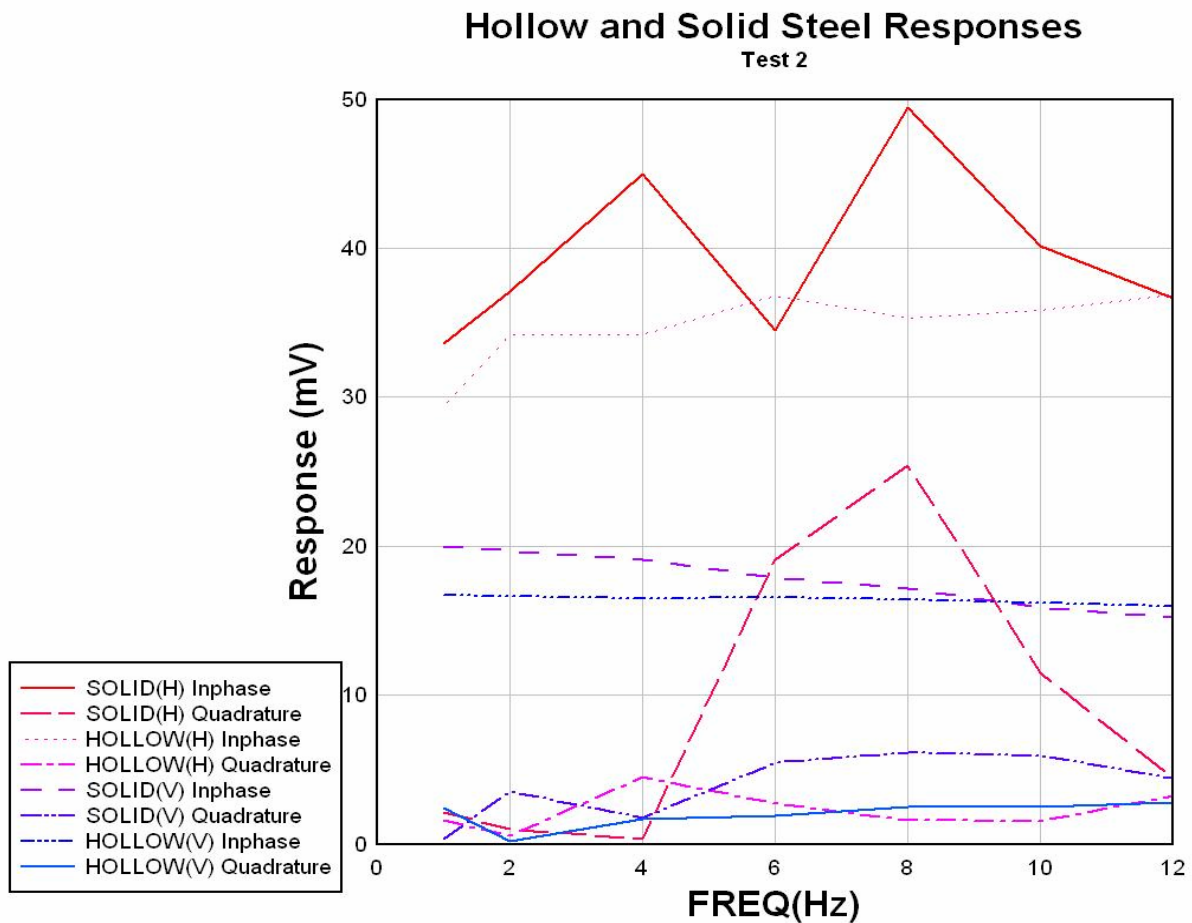


**Figure 21. Results from Test 2 using the hollow and solid steel test objects in vertical and horizontal orientations.**

Test 3 was conducted between 0.5 Hz and 8 Hz with the solid and hollow steel test objects in a horizontal orientation only. These data are shown in **Table 7** and graphically presented in **Figure 22**.

**Table 7. Data from the third experimental test setup**

FREQ (Hz)	SOLID		HOLLOW	
	Real	Imaginary	Real	Imaginary
0.5	35.0	7.5	32.0	2.1
1.0	41.5	6.4	40.5	2.1
2.0	40.0	3.0	44.0	2.5
4.0	63.5	14.0	44.0	2.5
6.0	69.0	14.0	44.0	6.0
8.0	10.0	79.0	49.0	2.8

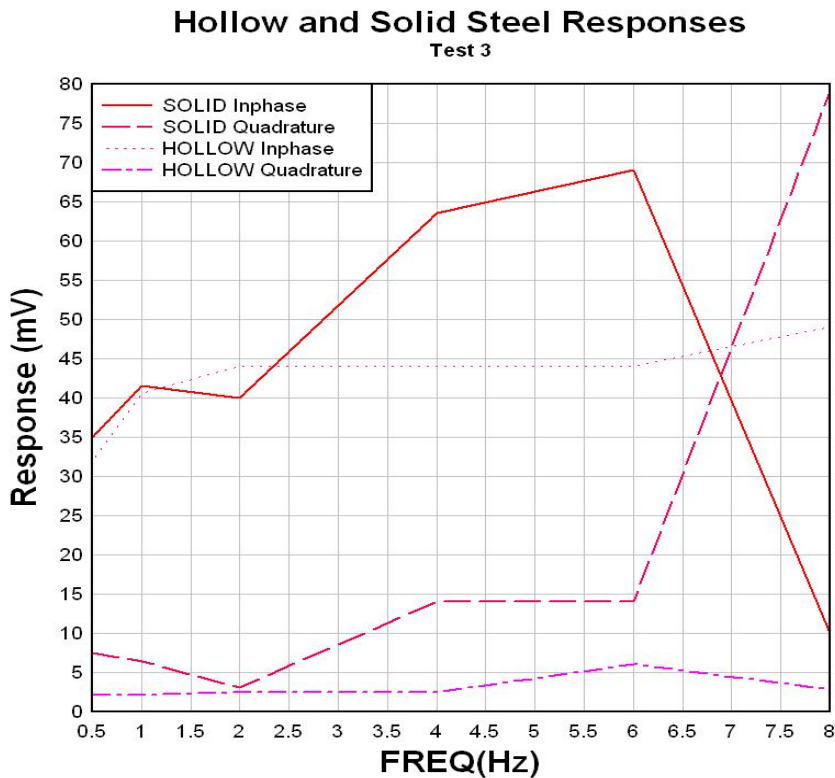


**Figure 22. Test 3 results of hollow and solid responses.**

A Geophex<sup>4</sup> GEM 3 system was also used to collect data from the same hollow and solid steel test objects. This setup is shown in **Figure 23**.



**Figure 23. The GEM 3 sensor is shown mounted above the solid steel test object.**

The GEM data were integrated with the rotating coil data and the joint overall responses are shown below in Figures 24 and 25.

We have incorporated the data from all three sets of experimental measurements made with the spinning transmitter instrument into the single presentations in Figures 24 and 25. Because the GEM readouts are in ppm we had to adjust the two datasets vertically to join them smoothly together. Data values (Inphase and Quadrature) acquired from the spinning transmitter were multiplied (scaled) by a factor of 100, for Inphase the multiplier was -100 while for Quadrature it was +100. Polarity (phase) is strictly arbitrary. Inphase data was then shifted (offset) by adding (or subtracting) an absolute value from each data point. This absolute value was determined by extrapolating the GEM Inphase data down to 12 Hz and determining the offset between that response and the rotating coil response at 12 Hz.

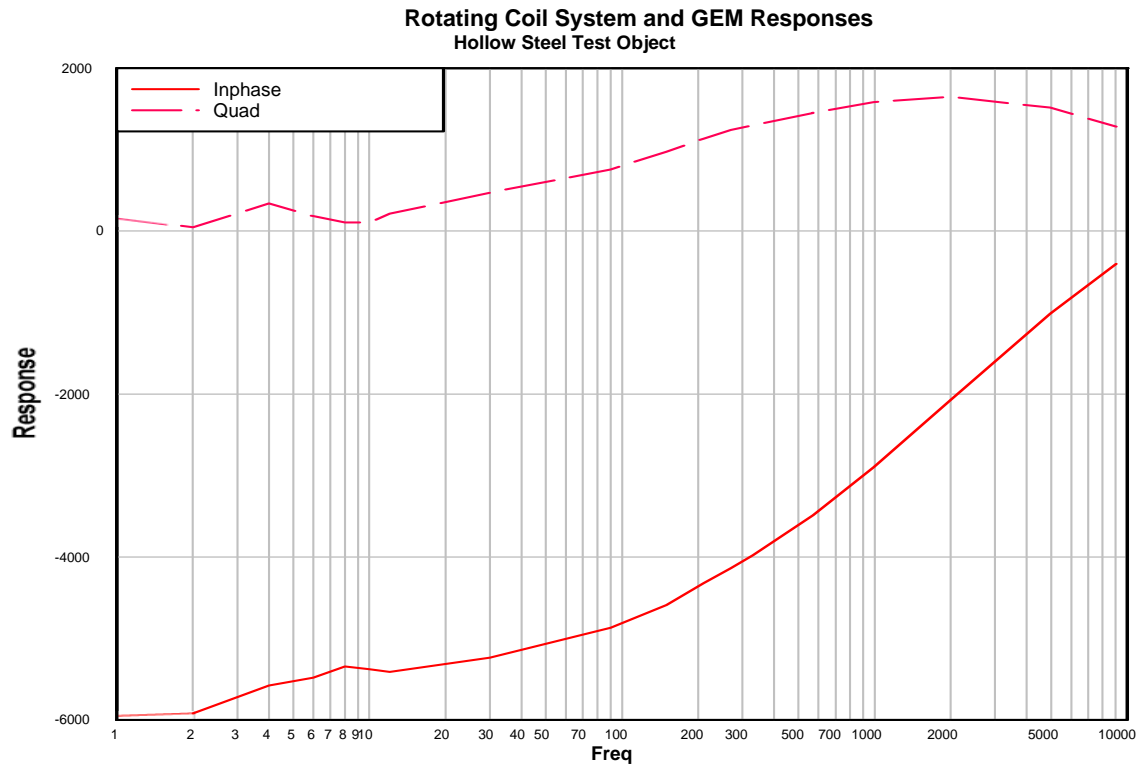


**Figure 24. Rotating coil system and GEM responses for the hollow steel test object.**

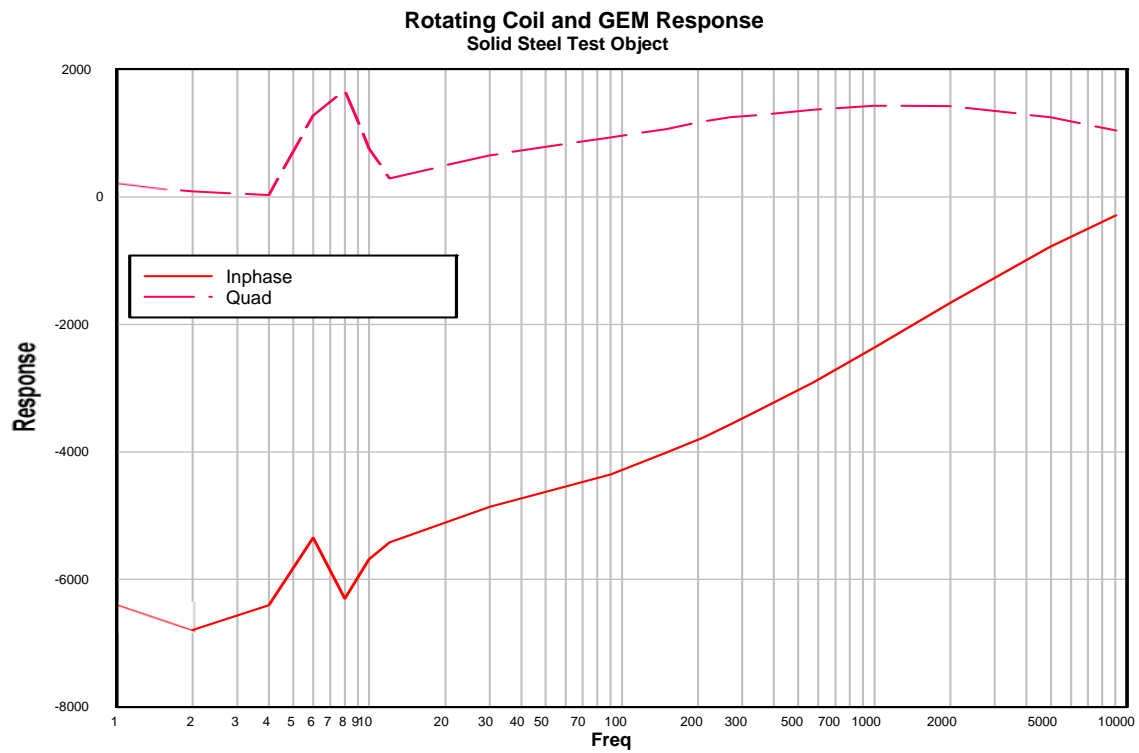


**Figure 25. Rotating coil system and GEM responses for the solid steel test object.**

## *Experimental Observations and Conclusions*

The inphase (in particular) and the quadrature measurements on each of the test objects as a function of frequency are not smoothly varying functions as we typically see from similar plots made with frequency-domain EM instruments. In our setup and testing of the spinning transmitter instrument, the instrumental measurements made without the test objects present are very stable both in time and as the spinning rate of the transmitter coil is increased or decreased. The spinning coil was slightly unstable at the highest frequencies because the platform was not exactly balanced. At the lower rates where we took data, it spun smoothly.

When one of the test objects is in place in its jig, each individual set of measurements that we made was quite stable and reproducible until the experiment was set up from scratch again. The coils were securely strapped down in their jigs and were relatively stable, but the test fixture was (by no means) rigidly constructed to maintain a highly precise relative positioning of the components.

We were convinced while the measurements were being made that there were legitimate maxima and minima in the inphase and quadrature measurements as a function of frequency. When they were graphically compared after the experiments were completed, we saw that the maxima and minima were similar from experiment to experiment, but did not occur at precisely the same frequencies in each experiment. It is unclear whether these apparent maxima and minima are completely experimental artifacts (noise) or whether they are partially (or entirely) associated with irregularities in the test objects.

The fact that our data from the spinning transmitter instrument and the GEM 3 smoothly join together and that their trends are consistent justifies and validates our approach in the design and construction of the instrument.

It would be both gratifying and informative to repeat these experiments with much better test objects and with a spinning transmitter experimental test platform that was much more rigidly constructed. However, the available funding and time constraints of the project allowed only for the construction of the bench top demonstration unit. The selection of the COTS system components and the design and construction of the required system electronics would form the basis for building a more capable prototype.

## 8. Summary

A complete basic Electromagnetic instrument utilizing a rotating transmitter coil to produce extremely low frequency (ELF) magnetic fields was designed, developed and tested. The basic concept was fully validated. A novel method of measuring the transmitter coil rotation and synchronizing it to the receiver coil signals was developed to produce a reference signal for the detection system. It was shown that the primary field can be cancelled well below -90 db by using two receiver coils connected in opposition. This achievement could likely be significantly improved in a more rigidly-fixed prototype. The detection system consisted of a digital signal processor (DSP) lock-in amplifier preceded by a special low frequency pre-amplifier designed and built for this application.

The system performance parameters were modeled using a sophisticated electromagnetic software modeling utility, and verified by making measurements with a single receiver. Once all parameters were verified and the second receiver coil was installed, two similar test objects (one hollow and one solid) were used to evaluate the system performance. These secondary magnetic fields induced in the test objects were measured and processed by the DSP lock-in amplifier and presented as Inphase and Quadrature results. These Inphase and Quadrature results from the EM system were recorded as a function of frequency between 0.5 and 12 Hz. A GEM 3 instrument was then used to collect data from 30 Hz up to 10 KHz and the two systems' data were joined producing one continuous response function from 1 Hz up to 10 KHz.

## 9. Future Research

Future research could involve taking this project’s design two steps further. The first modification would be achieved by designing the transmitter coil to transmit either a DC or a sinusoidal time-varying magnetic field. Operation using a sinusoidal-varying field would be achieved similarly to the commercial Frequency Domain (FD) EMI systems currently in use.

The second modification that we propose to make is to enhance the discrimination capabilities of the new FD EMI system by rotating the complete FD EMI assembly, including both the transmitter and receiver coils. This would allow us to create the “multiple looks” required to achieve accurate EM inversions. Refer to **Figure 26** for an explanation of this technique.

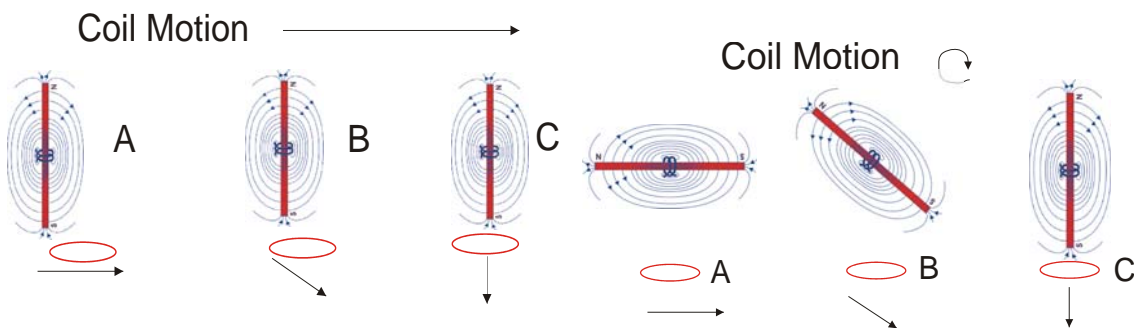


**Figure 26. Comparison of multiple excitation angles of the primary magnetic field. Left side: Measurements are achieved by laterally traversing the sensor over the target while keeping the coil oriented horizontally to the target (red circle). The lower arrow shows the major component of the transmitted field observed by the target. On the Right Side the positions of both the sensor and the target remain fixed. The transmit and receive coils are rotated together above the target. The lower arrows again show the field observed by the target.**

It has been shown both in physical measurements and in modeling studies that positional errors as small as 1 cm have serious detrimental effects on the quality of the inversion results. The proposed sensor described above would inherently remove all these positional discrepancies. We would use only one physical setup position to acquire the full bandwidth of data, incorporating the multiple excitation angles of the primary field that are necessary for the EM inversion. The proposed FD EMI system can be rotated step-wise to any number of angular positions to acquire complete EMI Inphase and Quadrature readings with the necessary transmitter coil (primary field) angular information. These three features; ELF, large bandwidth (1 Hz – 1 KHz), and a stationary multi-dimensional primary field will provide a significantly-improved capability to make the precise measurements required to discriminate intact UXO from clutter objects.

## References

1. K. O'Neill, S. Haider, F. Shubitidze, K Sun, C.O. Ao, H. Braunisch, and J.A. Kong, Ultra-wideband Electromagnetic Induction Spectroscopy
2. Hans Michlmayr, Magnetic Antennae for ULF, Detection and recording of Schumann resonances and other electromagnetic phenomena at frequencies below 50 Hz. June 2001
3. Perkin Elmer Instruments, Technical Note TN 1000, What is a Lock-in Amplifier
4. Geophex Instruments Ltd, 605 Mercury St., Raleigh, NC 27603

# Appendix A — DC Motor Control System Specifications

## Specifications

<b>Product Line</b>	VEXTA ®
<b>Motor Type</b>	Brushless DC
<b>Motor Frame Size</b>	3.54 in. sq.
<b>Output Power HP (W)</b>	1/8 HP (90W)
<b>Power Supply</b>	Single-Phase 100-115 VAC
<b>Gear/ Shaft Type</b>	Round Shaft
<b>Variable Speed Range (r/min)</b>	100 ~ 2000
<b>Rated Torque (lb-in)</b>	3.9
<b>Permissible Load Inertia</b>	32 oz-in <sup>2</sup>
<b>Available to Ship</b>	7 Business Days (1-5 pcs)
<b>Components</b>	AXUM590-A (Motor) AXUD90A (Control Unit)
<b>RoHS Compliant</b>	No
<b>Safety Standard</b>	UL CE CSA EN
<b>CE Marking</b>	Low Voltage Directives EMC Directives

<b>Acceleration/Deceleration Time</b>	0.5 ~ 10 sec. (at 2000 r/min with no load) set by a potentiometer.
<b>Control System</b>	Speed potentiometer on front panel.
<b>Insulation Class</b>	Class E (248°F [120°C])
<b>Insulation Resistance</b>	[Motor] 100 M ohms or more when 500 VDC is applied between the windings and the frame. [Control Unit] 100 M ohms or more when 500 VDC is applied between the power supply input terminal and the ground terminal, and between the power supply input terminal and the I/O terminal.
<b>Dielectric Strength</b>	[Motor] Sufficient to withstand 1500 VAC at 50 Hz applied between the windings and the frame. [Control Unit] Sufficient to withstand 1.8 kVAC at 50 Hz applied between the ground terminal and the power supply input terminal for 1 minute, and 3 kVAC at 50 Hz applied between the ground terminal and the I/O terminal for 1 minute.
<b>Ambient Temperature Range</b>	[Motor] 32°F ~ 122°F (0°C ~ 50°C), nonfreezing [Control Unit] 32°F ~ 104°F (0°C ~ 40°C), nonfreezing
<b>Ambient Humidity</b>	85% maximum (noncondensing)
<b>Operating Atmosphere</b>	No corrosive gases or dust
<b>Degree of Protection</b>	[Motor] IP65 (except for mounting surface) [Control Unit] IP10